DOI: https://doi.org/10.20372/star.V14.i3.11



ISSN: 2226-7522 (Print) and 2305-3372 (Online) Science, Technology, and Arts Research Journal Sci. Technol. Arts Res. J., July-Sep. 2025, 14(3), 134-143 Journal Homepage: https://journals.wgu.edu.et

Original Research

Investigation of Structural, optical, and Magnetic Properties of Ytterbium- Aluminum ions co-doped bismuth ferrite nano-Ceramics

Department of Physics, College of Natural and Computational Sciences, Wollega University,
Nekemte, Ethiopia

Abstract Article Information Article History: Received: 28-05-2025 Yb^{3+} ions co-doped bismuth ferrite (BFO) nanoparticles made using the sol-gel method. X-ray (XRD) analysis revealed the production of a single-phase perovskite structure, with decreasing average crystallite size as the concentration of co-dopants increased. The inherent ionic radii mismatch inhibits grain formation, resulting in a reduction in size. The diffuse reflectance spectroscopy Article History: Received: 28-05-2025Revised: 20-08-2025Accepted: 28-09-2025Keywords: Ytterbium- Aluminum, Sol-gel, Nano ceramics,

as the concentration of co-dopants increased, which is attributed to the introduction of a new energy level in the forbidden region, optimizing visible light absorption. Furthermore, the vibration sample magnetometer (VSM) results revealed a significant increase in saturation magnetization from 1.239 emu/g to 3.156 emu/g. This considerable magnetic increase is explained by the presence of co-dopants (Al³+ and Yb³+) in the host material, which effectively suppresses the natural cycloidal spiral spin structure that causes non-zero net magnetization. These results confirmed that the partial substitution of the co-dopants strategy has effectively tailored the properties of the pristine BFO, making the resulting nanoparticles promising candidates for the application in photocatalysis, magnetic memory storage, MRI contrast agents, and targeted drug delivery.

(DRS) revealed a decrease in optical band gap energy from 2.111 eV to 2.022 eV

Copyright @ 2025 STAR Journal, Wollega University. All Rights Reserved.

*Corresponding Author:

Bismuth ferrite, XRD

Senbeto Kena

E-mail:

senbkena@gmail.com

INTRODUCTION

Bismuth Ferrite (BFO) possesses ferromagnetism, ferroelectricity, and ferro elasticity in one phase. Ferrite has a G-type anti-ferromagnetic below 643 K Neel temperature and ferroelectric Curie temperature of 1103 K (Rhaman et al., 2024; Kharbanda et al., 2023; Smith et al., 2023). BFO is ferromagnetic iron ions because have uncompensated 3d orbitals. The space group of BFO's rhombohedral perovskite structure is R3c at room temperature (Senbeto & Elangovan, 2024; Ma et al., 2023). Certain techniques like coprecipitation, sol-gel, hydrothermal, sono chemical, solvothermal, and solid-state reaction

recommended for the synthesis of BFO (Mhamad et al., 2022; Sun et al., 2023). Due to its magnetic characteristics, BFO is attracting attention for telecommunications applications. These features improve magnetic hard drive and storage disk performance and storage capacity. nanoparticles can detect magnetic fields as magnetic sensors (Junaid et al., 2023; Sharma et al., 2023). Bismuth ferrite nanoparticles can improve light signals in optical communication systems, switches, and filters (Preethi & Ragam, 2021; Masoudpanah et al., 2017). Bismuth ferrite nanoparticles can carry pharmaceuticals if pure

Senbeto & Kebede

BFO contains the appropriate proportion of rare earth ions. Drug-loaded nanoparticles target specific cells and tissues. Bismuth-based compounds are also utilized as MRI contrast agents. They improve the detail and sensitivity of MRI images, which are used to diagnose and treat many health concerns, including photothermal therapy to kill cancer cells (Shahbazi et al., 2020; Petrukhin et al., 2024). Bismuth-based nano ferrites are promising photocatalysts. In these devices, nanoparticles deposited on a substrate and exposed to light transform light energy into chemical energy. Chemical energy can power water and air purification (Naveena et al., 2021; Wrzesińska et al., 2021).

Statement of the problem

The practical application of pure Bismuth Ferrite (BiFeO₃ or BFO) as a room-temperature multiferroic is severely limited by two inherent material deficiencies. First, a high electrical leakage current, driven primarily by point defects like oxygen vacancies, drastically compromises its ferroelectric performance and reliability. Second, its magnetic behavior is negligible due to a long-period cycloidal spiral spin structure that yields the Fe³⁺ magnetic moments to slightly zero net magnetization, which is unsuitable for magnetoelectric devices.

To mitigate these limitations, this study investigates the strategy of co-doping BFO with Ytterbium, Yb³⁺, and Aluminum Al³⁺ ions. The objective is to use the dopants to disrupt the detrimental spiral spin structure, thereby enhancing the material's magnetic moment by releasing its latent magnetization. Simultaneously, the co-doping is anticipated to manage the defect chemistry, suppressing the electrical leakage current and thus improving the overall multiferroic properties for advanced device applications.

Research Questions

1. How does co-doping with Ytterbium and Aluminum affect the crystal structure, purity, and dimensions of bismuth ferrite nano-ceramics?

Sci. Technol. Arts Res. J., July. -Sep, 2025, 14(3), 134-143

- 2. How does Ytterbium-Aluminum co-doping affect the optical band gap of the material, and how are these changes linked to its structural modifications?
- 3. How does co-doping influence the magnetic properties of the nano-ceramics, and does it enhance ferromagnetism by disrupting BFO's spin cycloid structure?

MATERIALS AND METHODS

For the synthesis of Al3+ and Yb3+ ions co-doped Bismuth Ferrite nanoparticles, the sol-gel method was employed. First, weighed stoichiometry ratio of metal nitrates Bi(NO₃)₃·5H₂O, Al(NO₃)₃·9H₂O, and Fe(NO₃)₃·9H₂O with purity over 99% as beginning materials. To prepare the baseline sample, 98 mole percent Fe(NO₃)₃·9H₂O and 2 mole percent Al(NO₃)₃·9H₂O are mixed in a 150 ml beaker containing an amount of doubly deionized water under vigorous stirring. An equal mole of Citric Acid (C₆H₈O₇) with the total mole of metal nitrates was introduced as a reaction facilitator, followed by drop-wise addition of ammonia solution to adjust pH-7. The mixture was stirred using a magnetic stirrer to form a transparent sol, which then became a highly viscous gel. This gel was subsequently dried at 210 °C into a soft ash, which was finely ground using an agate mortar and then pre-sintered (calcined) at 700 °C for 3 hours to decompose organic remnants and begin phase formation.

After cooling, the pre-sintered powder was thoroughly ground again and split into two portions for final preparation and characterization. The first portion was pelletized into a mold of 10 mm in diameter, 1.2 mm thick, using a 12.5-ton hydraulic press—these pellets would typically be sintered again for electrical testing. The second portion was held in an alumina crucible and subjected to a final densification step at 800 °C for 5 hours. This final sintered powder was used for comprehensive analysis: EDX spectroscopy confirmed the elemental composition, UV-Vis spectroscopy measured the optical properties, and VSM measurement was employed to determine the

Senbeto & Kebede
magnetic characteristics, specifically
magnetization-field behavior.

Characterization Techniques

A sample's crystal structure was characterized using X-ray diffraction. A room temperature, X'pert3 PRO diffractometer with Cu Kα radiation $(\lambda = 1.542 \text{ Å})$ was used for analysis. To collect Xray reflections, a detector was used with a Bragg's angle of 2θ from 10° to 70°, a goniometric radius of 240 mm, and a generator set to 40 kV and 30 mA. The sample's surface morphology was studied using a scanning electron microscope, JSM-7610F. The elemental composition of the sample was determined using an energy-dispersive X-ray spectrometer (EDX or EDS). Energy from this attachment removes a core electron, creating a vacancy. Spectrum peaks from electron excitation represent the sample's elemental composition. The magnetic characteristics were measured with a LAKESHORE VSM-7410 VSM, while the optical parameters were examined using diffused reflectance data from UV-Vis (Model: Shimadzu UV-1800) spectroscopy.

Theory

Various parameters can be determined by using the following equations,

$$D = \frac{k\lambda}{\beta Cos\theta} \tag{1}$$

Where D is the average crystallite size, k is the Scherer Constant, λ is the x-ray wavelength, β is the full width at half maximum (FWHM) of the diffraction peak, and θ is the Bragg angle for the measured peak.

$$\frac{1}{d_{hkl}^2} = \frac{4}{3} \left(\frac{h^2 + k^2 + hk}{a^2} \right) + \frac{l^2}{c^2} \tag{2}$$

The symbol, d_{hkl} , represents the interplanar spacing, which is the distance between two adjacent, parallel planes in a crystal lattice.

Sci. Technol. Arts Res. J., July. –Sep, 2025, 14(3), 134-143

$$2d_{hkl}Sin\theta = n\lambda \tag{3}$$

$$V = \frac{\sqrt{3}}{2}a^2c \tag{4}$$

Structural stability of the perovskite family, like Bismuth Ferrite (BiFeO), was predicted using the Goldschmidt Tolerance Factor (t), and is computed as follows:

$$t = \frac{(\langle R_A \rangle + R_0)}{\sqrt{2}(\langle R_B \rangle + R_B)}$$
 (5)

Where, R_A, R_B, and R_O are the average ionic radii of A-site, B-site, and Oxygen, respectively.

X-ray density of the sample was determined using equation (6):

$$\rho_{x-ray} = \frac{nM}{N_A V} \tag{6}$$

n stands for the number of atoms per unit cell in the compound, M is for the total molecular weight of the sample, N_A is an Avogadro number, and V is a volume of the unit cell.

RESULTS AND DISCUSSION

Results

Crystal Analysis

Figures 1(a-c) depicted the XRD pattern of the syntheses powder that definitively confirmed the successful formation of a single-phase material. Detailed investigation was conducted using Rietveld refinement using Full Prof software, which verify perovskite crystal structure with the space group R3c. This finding is in perfect agreement with the reference crystallographic data for BiFeO₃ (CIF no. 2102911) (Palewicz et al., 2007). Characteristic XRD peaks corresponding to the primary crystallographic planes of bismuth ferrite, including (012), the split (104)/(110) doublet, (024), (122), (018), (214), (208), and (220), were precisely identified. These peaks matched their expected Bragg's angles, 20 at 22.4°, 31.8°, 39.5°, 45.6°, 51.6°, 57.2°, 62.6°, and 67.0°.

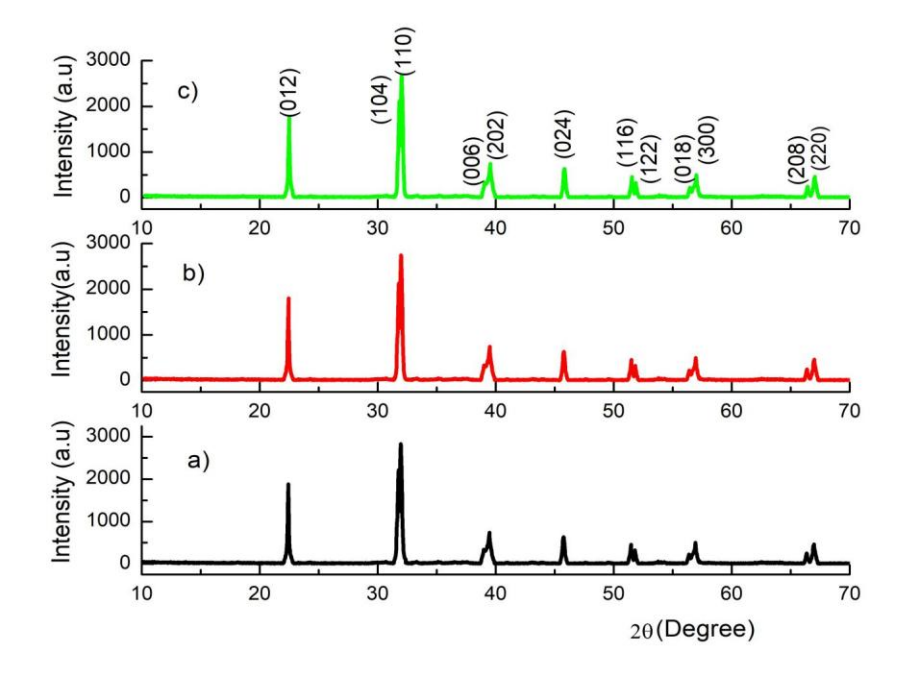


Figure 1. XRD pattern of $Bi_{1-x}Yb_xFe_{0.98}Al_{0.02}O_3$ samples for a) x=0.00, b) x=0.03, and c) x=0.06

Crucially, a systematic observation revealed that the most intense diffraction peaks slightly shift to higher Bragg's angles, 2θ with co-dopants. This shifting is due to the successful substitution of the

larger parent ions Bi³⁺ and Fe³⁺ by the smaller Yb³⁺ and Al³⁺ dopant ions, which results in lowering the crystallite size and lattice constants.

Table 1Crystal lattice parameters calculated from XRD data

Sample	Tolerance factor, t	Crystallite size, D(nm)	Lattice parameter			x-ray
			a=b	C	V	density,
			(nm)	(nm)	(nm^3)	(g/cm^3)
BiFe _{0.98} Al _{0.02} O ₃	0.887	37.451	0.5587	1.375	0.3717	6.97
$Bi_{0.97}Yb_{0.03}Fe_{0.98}Al_{0.02}O_3$	0.884	33.365	0.5575	1.364	0.3671	7.04
$Bi_{0.94}Yb_{0.06}Fe_{0.98}Al_{0.02}O_3$	0.881	28.853	0.5564	1.345	0.3606	7.14

Refined values of final crystal parameters, listed comprehensively in Table 1, were calculated based on the conspicuous (104)/(110) reflection doublet, utilizing established structural analysis equations (1)– (4) (Kumar et al., 2024; Devesa et al., 2020; Rhaman et al., 2019).

Discussions

The study successfully implemented a co-doping strategy involving doping of Ytterbium (Yb³⁺) into the Bi³⁺ site and Aluminum (Al³⁺) into the Fe³⁺ site.

The primary structural consequence of this dual substitution is a systematic contraction of the crystal lattice, as demonstrated in Table 1. The ionic radii of the dopants are significantly smaller than those of the host ions they replace $(r_{Yb}3+=0.086 \text{ nm} < r_{Bi}3+=0.117 \text{ nm}$ and $r_{Al}3+=0.054 \text{ nm} < r_{Fe}3+=0.065 \text{ nm}$). The cumulative effect of these smaller ionic radii throughout the structure imposes a contractive force on the perovskite framework, confirming that the co-dopants were successfully incorporated into the pure BiFeO₃ lattice.

Senbeto & Kebede

A second and more critical structural observation is the decrease in the Goldschmidt tolerance factor (t) with increasing co-dopant concentration. The tolerance factor predicts the stability and ideal geometry of the perovskite structure; values significantly below t=1 indicate high structural deformation. The observed decrease in t signifies a growing structural deformation and an increased departure from the ideal cubic symmetry. Specifically, this suggests an enhancement of the native rhombohedral distortion (Space Group R3c) inherent to BiFeO₃. This manipulation of the crystal lattice is highly significant because the magnitude of the lattice distortion is often directly correlated with the crystal structure stability and suppression of long-period spiral spin structure. These findings are strongly supported by established scientific

Sci. Technol. Arts Res. J., July. –Sep, 2025, 14(3), 134-143 literature, as referenced by W. Ben Taazayet et al. (2023), validating the controlled co-doping approach as an effective method for precisely tuning the fundamental structural properties of bismuth ferrite, a necessary prerequisite for improving its functional multiferroic behavior.

Morphological Studies

Figure 2 displays a synthesized sample SEM micrograph. The image shows agglomerated, homogenous grains. Yb³⁺-Al³⁺ ions and bismuth ferrite exhibit repulsive electrostatic, chemical, and magnetic interactions, resulting in nanoparticle alignment that reduces system energy (Nazeer et al., 2023).

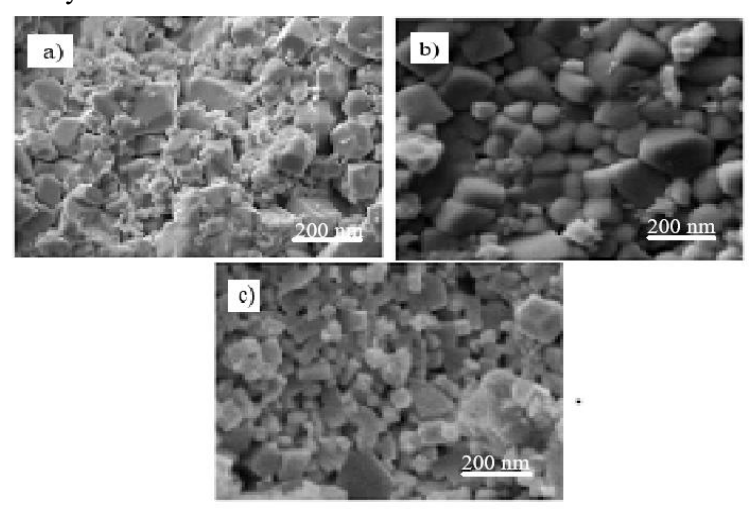


Figure 2. SEM micrograph image of $Bi_{1-x}Yb_xFe_{0.98}Al_{0.02}O_3$ samples for a)x=0.00, b) x=0.03, and c) x=0.06

Elemental Analysis

Sample energy dispersive X-ray spectroscopy data are shown in Figures 3 (a-c). The chemical included

all anticipated elements and no impurities, according to EDX analysis. Each sample element's atomic and weight percentages are listed in Table 2.

Table 2Elemental composition for $Bi_{1-x}Yb_xFe_{0.98}Al_{0.02}O_3$ sample

Element	x=0	x=0 x=0.03		x=0.06		
	At%	Wt%	At%	Wt%	At%	Wt%
ОК	60.6	18.303	59.484	17.660	59.475	17.700
Fe L	18.817	18.469	19.376	18.695	19.375	18.741

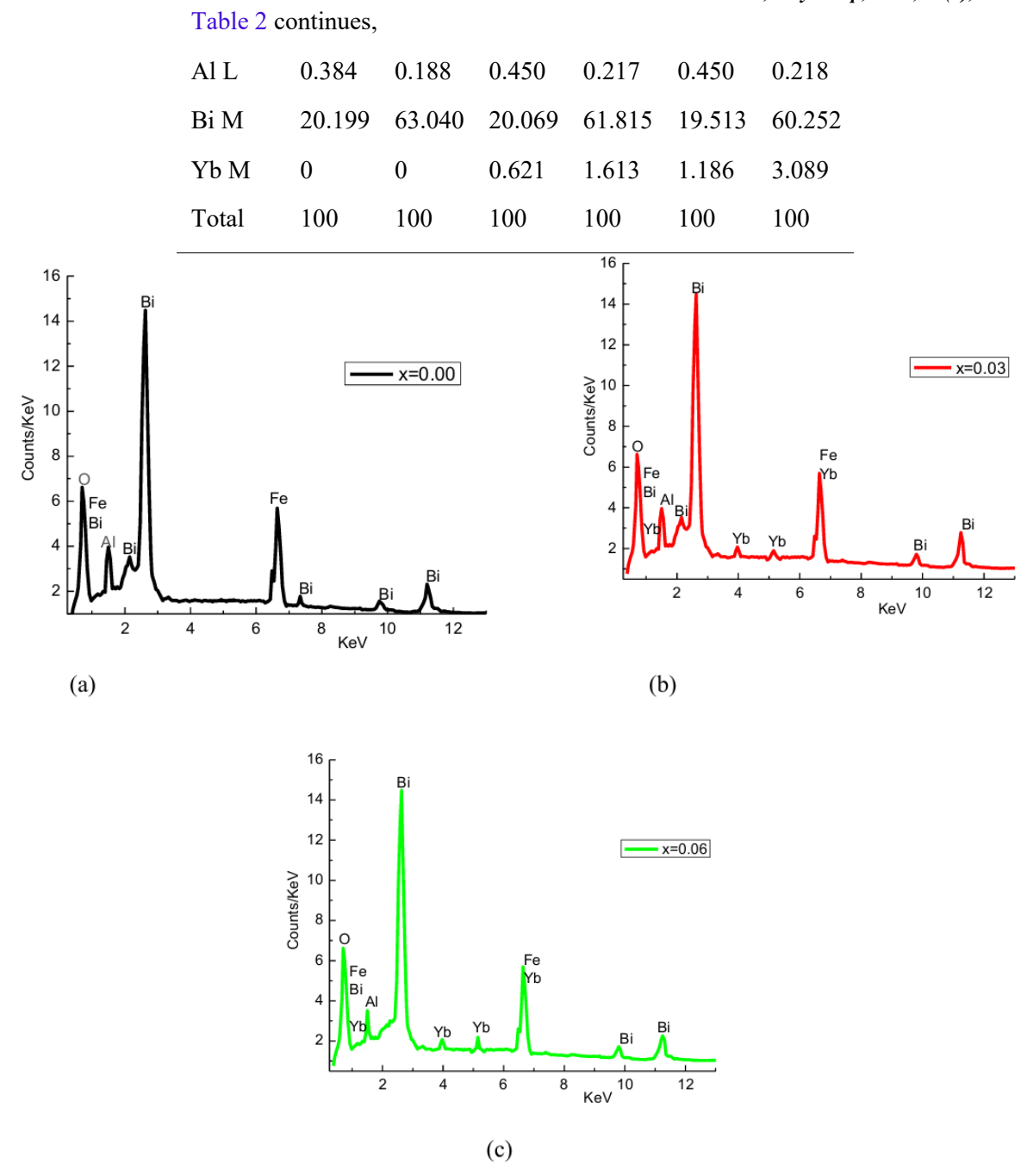


Figure 3. EDX spectra of $Bi_{1-x}Yb_xFe_{0.98}Al_{0.02}O_3$ samples for a) x=0.00, b) x=0.03, and c) x=0.06

Optical Studies

Figure 3 presents Tauc plot obtained from Diffuse Reflectance Spectroscopy (DRS) data Al³⁺ and Yb³⁺ co-doped BiFeO₃ nanoparticles. This technique used UV-Vis data acquired across the 250-800 nm wavelength range, for solid powdered samples to accurately estimate the optical band gap

energy (Eg) of the nanoceramics. This optical energy band gap of the sample can be found by applying the Kubelka-Munk function, defined as: (Rashidi et al., 2020; Lakshmi et al., 2021).

$$F(R) = \frac{k}{s} = \frac{(1-R)^2}{2R} \tag{7}$$

Where, $k = (1 - R)^2$ stands for absorption coefficient, R is the percentage reflectivity, called

Senbeto & Kebede reflectance obtained from DRS data, and s = 2R is the scattering factor.

By extrapolating in the Tauc plot of $(F(R).h\nu)^2$ vs $h\nu$, optical band gap energy was determined by intersecting to energy axis.

Sci. Technol. Arts Res. J., July. –Sep, 2025, 14(3), 134-143 As shown from the plot, the co-dopants lowered the energy band gap from 2.111 to 2.022 eV which is attributed to creation of new electronic state in the forbidden energy gap. Similar findings in Muthukrishnan et al. (2023) were obtained.

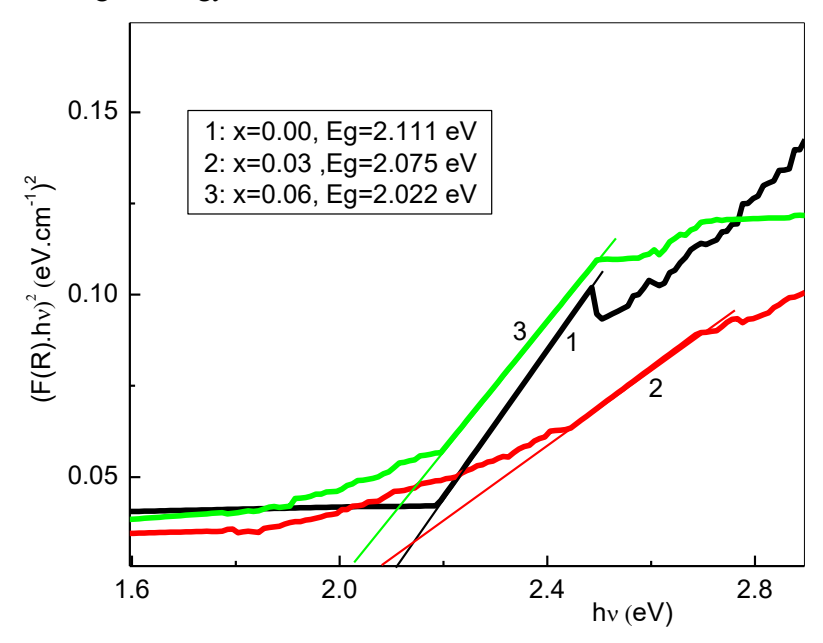


Figure 4. DRS analysis of $Bi_{1-x}Yb_xFe_{0.98}Al_{0.02}O_3$ samples for 1) x=0.00, 2) x=0.03, and 3) x=0.06

Magnetic Studies

Figure 5 displayed, a room temperature VSM measurement of Al³⁺ and Yb³⁺ ions co-doped BiFeO₃. The measurements were conducted up to maximum an applied field of 12000 Oe, providing insight into the material's magnetic response, including its saturation and hysteresis behavior. Table 3 shows the Co-doping Yb³⁺ and Al³⁺ ions to bismuth a ferrite nanoparticle enhances their

magnetic characteristics by suppressing spin spiral cycloidal G-type antiferromagnetic activity in the crystal structure. The decrease in the coercive field is generally associated with structural modifications and the size effects of the nanoparticles. These favorable results, particularly the enhanced magnetization achieved through spin structure manipulation, are consistent with similar strategies reported in scientific literature, such as the findings by Singh & Sharma (2019).

Table 3

Values of magnetic parameters with VSM

Sample	Mr (emu/g)	Ms (emu/g)	Hc (Oe)	Squareness (Mr/MS)
BiFe _{0.98} Al _{0.02} O ₃	0.471	1.239	1205.91	0.38
$Bi_{0.97}Yb_{0.03}Fe_{0.98}Al_{0.02}O_3$	0.825	2.533	446.63	0.32
$Bi_{0.94}Yb_{0.06}Fe_{0.98}Al_{0.02}O_3$	0.851	3.156	178.65	0.28

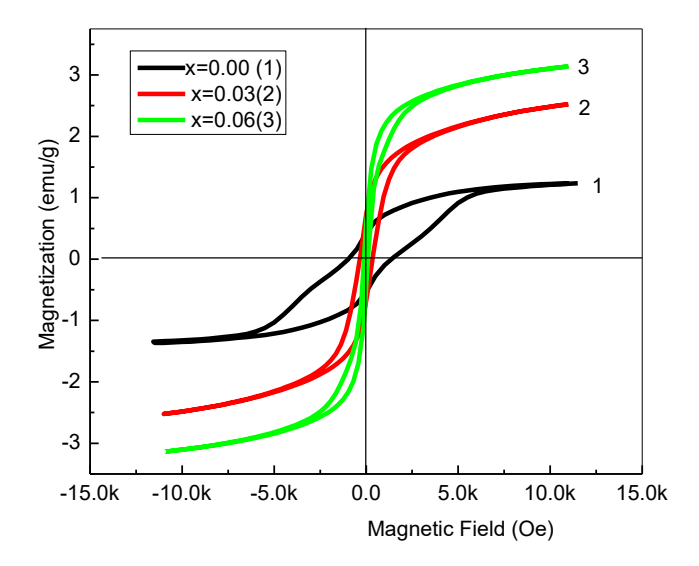


Figure 5. M-H loop for $Bi_{1-x}Yb_xFe_{0.98}Al_{0.02}O_3$ samples for 1) x=0.00, 2) x=0.03, and 3) x=0.06

CONCLUSION

Sol-gel synthesis technique for Yb³⁺ and Al³⁺ codoped bismuth ferrite nanoparticles was successfully employed. XRD analysis showed that the formation of single phase with an R3c space group, rhombohedral structure. The XRD analysis showed that the co-dopant's ionic radius mismatch with the compound's original ions reduced crystallite size from 37.451 to 28.853 nm because of the ionic radii mismatch of the Yb³⁺ and Al³ and Bi³⁺ and Fe³⁺ ions created an internal strain, which resulted in a decrease in the tolerance factor (from 0.887 to 0.881).

SEM images showed homogenous agglomerated particles distribution. EDX analysis revealed that all elements in their exact stoichiometric ratios, impurity-free. Diffuse reflectance spectroscopy (DRS) confirmed the reduction of the optical band gap energy from 2.111 to 2.022 eV, possibly due to new energy levels in BFO's forbidden area.

Vibrating sample magnetometer measurements showed improved magnetism. In contrast, codopants narrowed the hysteresis loop. Lower lattice constants reduced bismuth ferrite's spin spiral cycloidal G-type anti-ferromagnetism, improving its magnetic properties. This suppression induced spin canting and a net magnetic moment.

Recommendations

To fully realize the material's potential, subsequent research must concentrate on fine-tuning the synthesis process. Recommended ways include mapping out the effects of diverse doping levels, assessing how preparation variables affect structural qualities, like crystal size and void space, and moving beyond characterization to conduct thorough performance tests in relevant device applications such as photo catalysts or in magneto electric sensors.

Credit Authorship Contribution Statement

Senbeto Kena: Supervision, Conceptualization, Data Collection, Writing Original Draft

Kebede Legesse: Data Analysis, Validation. Review & Editing.

Conflict of Interest Statement

The authors affirm that there are no conflicts of interest associated with this publication.

Ethical Approval

Not applicable

Data Availability

The data supporting this study are available from the corresponding author upon reasonable request. Senbeto & Kebede

Acknowledgments

The authors extend their sincere gratitude to the Department of Physics, Wollega University for providing the necessary support to complete this study.

REFERENCES

- Devesa, S., Rooney, A., Graça, M., Cooper, D., & Costa, L. (2020). Williamson-hall analysis in estimation of crystallite size and lattice strain in Bi_{1.34}Fe_{0.66}Nb_{1.34}O_{6.35} prepared by the sol-gel method. *Materials Science and Engineering B*, 263, 114830. https://doi.org/10.1016/j.ms eb.2020.114830
- Junaid, M., Khan, M., Ain, N. U., Batoo, K. M., & Hussain, S. (2023). Electrical and magnetic characteristics of barium doped bismuth ferrite via sol–gel auto combustion technique. *Results in Chemistry*, 6, 101208. https://doi.org/10.1016/j.rechem.2023.101208
- Kharbanda, S., Dhanda, N., Sun, A. A., Thakur, A., & Thakur, P. (2023). Multiferroic perovskite bismuth ferrite nanostructures: A review on synthesis and applications. *Journal of Magnetism and Magnetic Materials*, 572, 170569. https://doi.org/10.1016/j.jmmm.2023.170569
- Kumar, A., Panigrahi, A., Shekhar, M., Kumar, L., & Kumar, P. (2024). Effect of Eu and Mn codoping on temperature dependent dielectric relaxation behaviour and electric conduction mechanisms of bismuth ferrite. *Journal of Electroceramics*, *52*(2), 144–169. https://doi.org/10.1007/s10832-024-00346-0
- Lakshmi, B., Thomas, B. J., & Gopinath, P. (2021). Accurate band gap determination of chemically synthesized cobalt ferrite nanoparticles using diffuse reflectance spectroscopy. *Advanced Powder Technology*, 32(10), 3706–3716. https://doi.org/10.1016/j.apt.2021.08.028
- Ma, Y., Shen, H., Fang, Y., Geng, H., Zhao, Y., Li, Y., Xu, J., & Ma, Y. (2023). Effect of bismuth on the structure, magnetic and photocatalytic characteristics of GDFEO3. *Magneto*

- Sci. Technol. Arts Res. J., July. –Sep, 2025, 14(3), 134-143 chemistry, 9(2), 45. https://doi.org/10.3390/magnetochemistry9020045
- Masoudpanah, S. M., Mirkazemi, S. M., Bagheriyeh, R., Jabbari, F., & Bayat, F. (2017). Structural, magnetic and photocatalytic characterization of Bi1–x La x FeO3 nanoparticles synthesized by thermal decomposition method. *Bulletin of Materials Science*, 40(1), 93–100. https://doi.org/10.1007/s12034-016-1346-0
- Mhamad, S. A., Ali, A. A., Mohtar, S. S., Aziz, F.,
 Aziz, M., Jaafar, J., Yusof, N., Salleh, W. N.
 W., Ismail, A. F., & Chandren, S. (2022).
 Synthesis of bismuth ferrite by sol-gel auto combustion method: Impact of citric acid concentration on its physicochemical properties. *Materials Chemistry and Physics*, 282, 125983. https://doi.org/10.1016/j.mat chemphys.2022.125983
- Muthukrishnan, R. M., Devee, D. R., Ansari, P. M. Y., Sivanesan, T., & Kader, S. M. A. (2023). Investigating the structural, optical and electrochemical performance of bismuth ferrite (BiFeO3) nanoparticles toward photocatalytic activity: as an effect of reducing agent. *Journal of Materials Science Materials in Electronics*, 34(6). https://doi.org/10.1007/s10854-023-09 8 77-8
- Naveena, G., Ravinder, D., Babu, T. A., Reddy, B. R., Sumalatha, E., Vani, K., Rajender, T., & Prasad, N. V. K. (2021). Low-temperature magnetic properties of erbium doped bismuth nano-ferrites. *Journal of Materials Science Materials in Electronics*, 32(13), 18224–18230. https://doi.org/10.1007/s10854-021-06365-9
- Nazeer, Z., Bibi, I., Majid, F., Kamal, S., Arshad, M. I., Ghafoor, A., Alwadai, N., Ali, A., Nazir, A., & Iqbal, M. (2023). Optical, photocatalytic, electrochemical, magnetic, dielectric, and ferroelectric properties of CD- and ER-Doped BIFEO3 prepared via a facile microemulsion route. *ACS Omega*, 8(28), 24980–24998. https://doi.org/10.1021/acsomega.3c01542
- Palewicz, A., Przeniosło, R., Sosnowska, I., & Hewat, A. W. (2007). Atomic displacements in

- Senbeto & Kebede
 BiFeO3 as a function of temperature: neutron diffraction study. Acta Crystallographica Section B Structural Science, 63(4), 537–544. https://doi.org/10.1107/s0108768107023956
- Petrukhin, D., Salnikov, V., Nikitin, A., Sidane, I., Slimani, S., Alberti, S., Peddis, D., Omelyanchik, A., & Rodionova, V. (2024). Effect of bismuth ferrite nanoparticles on physicochemical properties of polyvinylidene Fluoride-Based nanocomposites. *Journal of Composites Science*, 8(8), 329. https://doi.org/10.3390/jcs8080329
- Preethi, A. J., & Ragam, M. (2021). Effect of doping in multiferroic BFO: A review. *Journal of Advanced Dielectrics*, 11 (06). https://doi.org/10.1142/s2010135x21300012
- Rashidi, P., Ghamari, M., &Ghasemifard, M. (2020). The structural and optical band gap energy evaluation of nano TiO₂ powders by diffuse reflectance spectroscopy prepared via combustion method. *International Nano Letters.*, 10(4), 271–277. https://doi.org/10.1007/s40089-020-00313-x
- Rhaman, M., Miah, & Ahmad, T. (2024). Investigation of magnetic and electric properties of bismuth ferrite nanoparticles at different temperatures. *Nano-Structures & Nano-Objects*, *39*, 101304. https://doi.org/10.1016/j.nanoso.2024.101304
- Rhaman, M. M., Matin, M. A., Hossain, M. N., Mozahid, F. A., Hakim, M. A., & Islam, M. F. (2019). Bandgap engineering of cobalt-doped bismuth ferrite nanoparticles for photovoltaic applications. *Bulletin of Materials Science*, 42(4). https://doi.org/10.1007/s12034-019-1871-8
- Senbeto, E., & Elangovan, S. (2024). Structural, optical, and magnetic properties study of Dy-Cr co-doped bismuth ferrite (BFO) nanoparticles. *Results in Chemistry*,1018 55. https://doi.org/10.1016/j.rechem.2024.101 855
- Shahbazi, M., Faghfouri, L., Ferreira, M. P. A., Figueiredo, P., Maleki, H., Sefat, F., Hirvonen, J., & Santos, H. A. (2020). The versatile biomedical applications of bismuth-based

- Sci. Technol. Arts Res. J., July. –Sep, 2025, 14(3), 134-143 nanoparticles and composites: therapeutic, diagnostic, biosensing, and regenerative properties. Chemical Society Reviews, 49(4), 1253–321. https://doi.org/10.1039/c9cs00283a
- Sharma, S., Kumar, A., Thakur, O.P. (2023). Modified BiFeO₃ Perovskites: Investigations on their Structural, and Magnetic Properties. *Indian Journal of Engineering and Materials Sciences*;30: 729-734. https://doi.org/10.56042/ijems.v30i5.6899
- Singh, H. H., & Sharma, H. B. (2019). Investigation on electrical, magnetic and magneto-dielectric properties of yttrium and cobalt co-doped bismuth ferrite nanoparticles. *Indian Journal of Physics*, *94*(10), 1561–1572. https://doi.org/10.1007/s12648-019-01611-7
- Smith, L., Shield, J., Ahmadi, Z., Jeelani, S., &Rangari, V. (2023). Synthesis and characterization of bismuth ferrite particles using a nano-agitator bead mill. *AIP Advances*, *13*(3). https://doi.org/10.1063/5.013 2099
- Sun, H., Qin, P., Liang, Y., Yang, Y., Zhang, J., Guo, J., Hu, X., Jiang, Y., Zhou, Y., Luo, L., & Wu, Z. (2023). Sonochemically assisted the synthesis and catalytic application of bismuth-based photocatalyst: A mini review. *Ultrasonics Sonochemistry*, 100, 106600. https://doi.org/10.1016/j.ultsonch.202 3.106600
- Taazayet, W. B., Zouari, I. M., & Mliki, N. T. (2023b). Crystal field modification via rare earth ions (Dy, Nd) incorporation on BiFeO3 fine nanoparticles. *Journal of Materials Science Materials in Electronics*, 34(31). https://doi.org/10.1007/s10854-023-11487-3
- Wrzesińska, A., Khort, A., Witkowski, M., Szczytko, J., Ryl, J., Gurgul, J., Kharitonov, D. S., Łątka, K., Szumiata, T., & Wypych-Puszkarz, A. (2021). Structural, electrical, and magnetic study of La-, Eu-, and Er- doped bismuth ferrite nanomaterials obtained by solution combustion synthesis. *Scientific Reports*, 11(1). https://doi.org/10.1038/s41598-021-01983-z